Temporal and spectral effects of cross-phase modulation on copropagating ultrashort pulses in optical fibers

Govind P. Agrawal
The Institute of Optics, University of Rochester, Rochester, New York 14627

P. L. Baldeck and R. R. Alfano
Institute for Ultrafast Spectroscopy and Lasers and Photonics Application Laboratory, Department of Electrical Engineering and Department of Physics, The City College of New York, New York, New York 10031

(Received 31 October 1988)

The effects of cross-phase modulation (XPM) on the evolution of copropagating ultrashort pulses in an optical fiber are discussed theoretically by solving the coupled-amplitude equations which include the contributions of self-phase modulation, XPM, pulse walk-off, and group-velocity dispersion. A pump-probe configuration is studied to isolate the XPM effects. In the case of nondispersive XPM, the probe shape remians nearly unchanged while the probe spectrum exhibits asymmetric spectral broadening and a shift toward the red or the blue side depending on the initial pump-probe delay. In the case of dispersive XPM, the combination of group-velocity dispersion and XPM lead to both temporal and spectral changes. The new XPM-induced phenomena, optical wave breaking, and pulse compression are discussed in detail.

I. INTRODUCTION

When two optical pulses overlap inside a nonlinear medium, they can interact with each other through cross-phase modulation (XPM), a phenomenon that is always accompanied by self-phase modulation (SPM). In general, the two pulses can differ in their wavelengths as well as in their states of polarization. The well-known optical Kerr effect[1-3] belongs to this latter category. Its observation in optical fibers[4] may be considered the earliest manifestation of XPM. The case of two identically polarized pulses at different wavelengths has attracted considerable attention recently,[5-22] particularly from the standpoint of the effect of XPM on the pulse spectrum. Two cases must be distinguished here. In one case, the second pulse is generated internally through the gain provided by stimulated Raman scattering (SRS). In the other case, two pulses at different wavelengths are incident at the fiber input and interact through XPM without any energy transfer between them. The objective of this paper is to investigate this second case. More specifically, we study how the XPM-induced interaction can affect the pulse shapes and spectra in the presence of group-velocity dispersion (GVD) in optical fibers.

The effects of XPM on the pulse spectrum have been observed in bulk glasses[6] as well as in silica fibers.[9,10] In the case of optical fibers, a pump-probe configuration is often used[9,14] to isolate the XPM effects on the probe spectrum. When the probe pulse is launched simultaneously with an intense pump pulse, the probe spectrum is generally broadened and develops an oscillatory structure. This occurs because XPM imposes a frequency chirp on the probe pulse in a manner similar to that induced by SPM. In contrast with the SPM case, however, the probe spectrum can be symmetric or asymmetric depending on the initial delay between the pump and probe pulses. The origin of asymmetry can be understood by using a nonlinear phase-shift model that includes the walk-off effects.[9] Physically, the pump and probe pulses walk off from each other as a result of their slightly different group velocities. Such walk-off effects can lead to an XPM-induced frequency shift[14] of the probe spectrum.

In most of the pump-probe experiments in optical fiber the XPM produced spectral changes without a significant change in the pulse shape. These experiments were performed in the so-called nondispersive-XPM regime where the GVD effects were negligible during the XPM interaction except for the group-velocity mismatch. When the GVD effects are strong enough during the XPM interaction, both the shape and the spectrum of probe pulses are expected to be affected considerably by the presence of the pump pulses. As discussed in this paper, the novel nonlinear phenomena can take place in this dispersive-XPM regime. The XPM-induced modulation instability is one such phenomenon and has been discussed both theoretically[11] and experimentally.[15,16] Two other nonlinear phenomena discussed here are XPM-induced optical wave breaking[19] and XPM-induced pulse compression.[17-19]

The paper is organized as follows. In Sec. II we obtain the coupled-amplitude equations which govern the XPM interaction. Two length scales, known as the walk-off length L_W and the dispersion length L_D, are introduced to emphasize the relative importance of the walk-off and GVD effects. Section III considers the case of nondispersive XPM applicable when $L_W \ll L_D$. The coupled-amplitude equations can be solved analytically in this

case to obtain the frequency chirp imposed by the combined effects of SPM and XPM. The case of dispersive XPM, applicable when L_W and L_D are comparable, is discussed in Sec. IV with particular emphasis on optical wave breaking. Section V is devoted to the study of XPM-induced pulse compression. Finally, the results are summarized in Sec. VI.

II. COUPLED-AMPLITUDE EQUATIONS

In this section we obtain a set of two coupled-amplitude equations by including the effects of GVD, SPM, and XPM. Since details are available elsewhere,[23] we outline only the essential steps. We consider the case in which two optical pulses with nonoverlapping spectra are incident on a single-mode polarization-preserving fiber. Both beams are assumed to be linearly polarized along one of the principle axes of the fiber. The wave-propagation problem is then considerably simplified and can be solved by using the scalar wave equation

$$\nabla^2 E - \frac{1}{c^2}\frac{\partial^2}{\partial t^2}(\tilde{n}^2 E)=0 , \tag{2.1}$$

where E is the total electric field, c is the velocity of light in vacuum, and the refractive index $\tilde{n}$ is given by

$$\tilde{n}=n(\omega)+n_2|E'|^2 . \tag{2.2}$$

The GVD effects result from the frequency dependence of the linear part of the refractive index. The nonlinear effects are included through the parameter n_2 in Eq. (2.2). The frequency dependence of n_2 can generally be ignored. We have introduced in Eq. (2.2) a quantity E' related to E by $E'=(\epsilon_0 c/2n)^{1/2}E$ such that $|E'|^2$ represents the intensity (units W/m^2). For silica fibers the parameter $n_2=3.2\times10^{-20}$ m^2/W. We use mks units (SI) throughout the paper.

The total electric field associated with the two pulses can be written in the form

$$E'(x,y,z,t)=\mathrm{Re}\left[\sum_{j=1}^{2} F_j(x,y)A_j(z,t) \times\exp[ik_j z-\omega_j t)]\right] , \tag{2.3}$$

where ω_j is the optical frequency and $k_j=n_j\omega_j/c$ with $n_j=n(\omega_j)$. The complex amplitude $A_j(z,t)$ is assumed to be slowly-varying with respect to both z and t. The quantity $F_j(x,y)$ represents the transverse distribution of the fundamental fiber mode. It is generally different for the two pulses even in a single-mode fiber because of the difference in the center wavelengths $\lambda_j=2\pi c/\omega_j$ ($j=1$ or 2). By substituting Eqs. (2.2) and (2.3) in Eq. (2.1), expanding k_j in a Taylor series around ω_j, and making the slowly-varying-envelope approximation, the amplitudes A_1 and A_2 are found to satisfy the following equation:[23]

$$\frac{\partial A_j}{\partial z}+\frac{\alpha_j}{2}A_j+\frac{1}{v_{gj}}\frac{\partial A_j}{\partial t}+\frac{i}{2}\beta_j\frac{\partial^2 A_j}{\partial t^2} =\frac{in_2\omega_j}{c}(f_{jj}|A_j|^2+2f_{jk}|A_k|^2)A_j , \tag{2.4}$$

where $j,k=1$ or 2, $j\neq k$, the group velocity

$$v_{gj}=\left[\frac{dk_j}{d\omega}\right]^{-1}_{\omega=\omega_j} , \tag{2.5}$$

and the GVD coefficient

$$\beta_j=\left[\frac{d^2k_j}{d\omega^2}\right]_{\omega=\omega_j} . \tag{2.6}$$

The overlap integrals f_{jk} are defined by

$$f_{jk}=\int |F_j(x,y)|^2|F_k(x,y)|^2 dx\,dy , \tag{2.7}$$

where $F_j(x,y)$ is assumed to be normalized such that $\int |F_j(x,y)|^2 dx\,dy=1$. The second term in Eq. (2.4) is introduced phenomenologically to account for the fiber loss; α_j is the power-attenuation coefficient. The dimension of the envelope amplitude A_j has been chosen such that $|A_j|^2$ represents the power in the fiber mode. This specific choice is made to facilitate comparison between theory and experiment.

The propagation equation (2.4) is valid in the slowly-varying-envelope approximation. This approximation amounts to assuming that the spectral width of each pulse remains much smaller than its central frequency ($\Delta\omega_j \ll \omega_j$). It holds well for pulse widths ≥ 1 ps. For ultrashort pulses having width ≤ 100 fs it becomes necessary to include the contributions of higher-order nonlinear and dispersive effects. The higher-order dispersive effects can be included by adding a third-derivative term on the left-hand side of Eq. (2.4). The higher-order nonlinear effects are included by adding two additional terms resulting from self-steepening and nonlinearity relaxation. The latter is responsible for the soliton self-frequency shift and includes the contribution of stimulated Raman scattering.[24–26] These higher-order nonlinear effects are not considered in this paper.

Equation (2.4) can describe propagation in multimode fibers for the case in which the two pulses propagate in different fiber modes. In the case of single-mode fibers the differences among various overlap integrals are small and can be neglected in practice. With this approximation, the coupled-amplitude equations become

$$\frac{\partial A_1}{\partial z}+\frac{\alpha_1}{2}A_1+\frac{1}{v_{g1}}\frac{\partial A_1}{\partial t}+\frac{i}{2}\beta_1\frac{\partial^2 A_1}{\partial t^2} =i\gamma_1(|A_1|^2+2|A_2|^2)A_1 , \tag{2.8}$$

$$\frac{\partial A_2}{\partial z}+\frac{\alpha_2}{2}A_2+\frac{1}{v_{g2}}\frac{\partial A_2}{\partial t}+\frac{i}{2}\beta_2\frac{\partial^2 A_2}{\partial t^2} =i\gamma_2(|A_2|^2+2|A_1|^2)A_2 , \tag{2.9}$$

where the nonlinearity coefficient

$$\gamma_j=\frac{n_2\omega_j}{cA_{\mathrm{eff}}} , \tag{2.10}$$

and the effective core area is introduced by using $A_{\mathrm{eff}}=1/f_{11}$. Typically $A_{\mathrm{eff}}=10$–20 μm^2 in the visible region since the core diameter is 3–4 μm to ensure

single-mode operation. The corresponding values of γ_1 and γ_2 are in the range 20–30 W^{-1} Km^{-1} depending on the wavelengths of the incident pulses. The GVD coefficients β_1 and β_2 in the visible region are in the range 40–60 ps^2/km. In the infrared region extending from 1.3–1.6 μm, β_1 and β_2 are negative for silica fibers as the pulses experience anomalous GVD.

The two terms on the right-hand side of Eqs. (2.8) and (2.9) result from the fiber nonlinearity. The first term leads to SPM while the second term is responsible for XPM. The XPM term couples the two pulses; in its absence the two overlapping pulses would have copropagated without affecting each other. However, the XPM-induced mutual coupling may affect both the shape and the spectrum of each pulse. The important point is that such a coupling can occur irrespective of the wavelength difference between the two pulses. GVD can influence the XPM effects in two ways. First, it is responsible for a mismatch between the group velocities associated with the two pulses. As a result, the two pulses walk off from each other as they propagate along the fiber. The XPM interaction ceases to occur when the pulses are physically separated from each other. For a pulse of width T_0, one can introduce a walk-off length defined by

$$L_W=\frac{T_0}{|v_{g_1}^{-1}-v_{g_2}^{-1}|} . \tag{2.11}$$

XPM occurs only over distances $\sim L_W$ irrespective of the actual fiber length. L_W depends on the relative wavelengths and decreases as the wavelength difference $\Delta\lambda$ increases. Typically $L_W\sim 1$ m in the visible region for $T_0=10$ ps and $\Delta\lambda=10$–20 nm. The second effect of GVD comes through the second-derivative term in Eqs. (2.8) and (2.9). Since different spectral components of a pulse travel at slightly different speeds, the pulse shape and the spectrum acquire new features when SPM and XPM occur together with GVD. The relative importance of such GVD effects is governed by the dispersion length defined by

$$L_D=T_0^2/|\beta_1| . \tag{2.12}$$

For a 10-ps pulse $L_D\gtrsim 1$ km. If the fiber length $L\ll L_D$, the GVD effects are negligible. In the case of XPM, L_W governs the distance over which the two pulses interact with each other. The GVD effects are most dominant when L_W and L_D are comparable. This can occur for $T_0\lesssim 1$ ps.

To understand the qualitative features associated with XPM, it is convenient to define

$$T=t-z/v_{g_1},\quad \tau=T/T_0 . \tag{2.13}$$

The time τ is measured in a reference frame moving at the group velocity of pulse 1 and is normalized to the width T_0 of that pulse. The coupled-amplitude equations (2.8) and (2.9) then take the form

$$\frac{\partial A_1}{\partial z}+i\frac{\mathrm{sgn}(\beta_1)}{2L_D}\frac{\partial^2 A_1}{\partial\tau^2}=i\gamma_1(|A_1|^2+2|A_2|^2)A_1 , \tag{2.14}$$

$$\frac{\partial A_2}{\partial z}+\frac{\epsilon}{L_W}\frac{\partial A_2}{\partial\tau}+i\frac{\mathrm{sgn}(\beta_1)}{2L_D}\frac{\beta_2}{\beta_1}\frac{\partial^2 A_2}{\partial\tau^2}=i\gamma_2(|A_2|^2+2|A_1|^2)A_2 , \tag{2.15}$$

where $\epsilon=1$ or -1 depending on the sign of $v_{g_1}-v_{g_2}$, i.e., $\epsilon=\mathrm{sgn}(v_{g_1}-v_{g_2})$. The fiber loss has been neglected for simplicity. This is not a limitation since the fiber lengths commonly employed in the XPM experiments are such that $L\sim L_W$, and the fiber loss is negligible ($\alpha_j L\ll 1$ for $j=1$ and 2). Equations (2.14) and (2.15) are the basic propagation equations for the study of the XPM effects. In the next two sections we consider their solutions to see how XPM influences the shape and the spectrum of two copropagating optical pulses.

III. NONDISPERSIVE CROSS-PHASE MODULATION

In many experimental situations the dispersion length L_D is much larger compared with both L and L_W. The second-derivative terms in Eqs. (2.14) and (2.15) can then be neglected. This simplifies the problem considerably, and the resulting equations can be solved analytically. Since this case also leads to considerable physical insight, we consider it first. One can readily verify that the pulse shape does not change in the limit of infinitely large L_D. The general solution of Eqs. (2.14) and (2.15) is then given by

$$A_1(L,\tau)=A_1(0,\tau)\exp(i\phi_1) , \tag{3.1}$$

$$A_2(L,\tau)=A_2(0,\tau-\epsilon L/L_W)\exp(i\phi_2) , \tag{3.2}$$

where $\epsilon=\mathrm{sgn}(v_{g_1}-v_{g_2})$,

$$\phi_1(\tau)=\gamma_1 L\left[|A_1(0,\tau)|^2+\frac{2}{L}\int_0^L|A_2(0,\tau-\epsilon z/L_W)|^2dz\right] , \tag{3.3}$$

$$\phi_2(\tau)=\gamma_2 L\left[|A_2(0,\tau)|^2+\frac{2}{L}\int_0^L|A_1(0,\tau+\epsilon z/L_W)|^2dz\right] . \tag{3.4}$$

The physical interpretation is clear. The first term in Eqs. (3.3) and (3.4) is due to SPM. The second term has its origin in XPM. The XPM contribution changes along the fiber because of the group-velocity mismatch and is obtained by integrating over the fiber length.[9]

The integration in Eqs. (3.3) and (3.4) can be performed for specific pulse shapes. As an illustration consider the case of two unchirped Gaussian pulses of the same width T_0. The initial amplitudes are given by

$$A_1(0,\tau)=\sqrt{P_1}\exp(-\tau^2/2) , \tag{3.5}$$

$$A_2(0,\tau)=\sqrt{P_2}\exp[-(\tau-\tau_d)^2/2] , \tag{3.6}$$

where P_1 and P_2 are the incident peak powers and τ_d is the initial delay between the two pulses. By using Eqs. (3.3)-(3.7), the nonlinear phase ϕ_1 is given by

$$\phi_1(\tau)=\gamma_1\{P_1 L \exp(-\tau^2) + \epsilon P_2 L_W \sqrt{\pi}[\mathrm{erf}(\tau-\tau_d) - \mathrm{erf}(\tau-\tau_d-\epsilon L/L_W)]\} . \quad (3.7)$$

A similar expression is obtained for ϕ_2.

A time dependence of the phase is equivalent to a frequency chirp induced by SPM and XPM. Such a chirp leads to spectral broadening of the pulses. An expression for the frequency chirp is obtained by using the definition

$$\Delta\nu_j(\tau)=-\frac{1}{2\pi T_0}\frac{\partial\phi_j}{\partial\tau} \quad (j=1 \text{ or } 2) . \quad (3.8)$$

By using Eqs. (3.7) and (3.8) the chirp is given by

$$\Delta\nu_1(\tau)=\frac{\gamma_1}{\pi T_0}[P_1 L\tau e^{-\tau^2} - \epsilon P_2 L_W (e^{-(\tau-\tau_d)^2} - e^{-(\tau-\tau_d-\epsilon L/L_W)^2})] . \quad (3.9)$$

The expression for $\Delta\nu_2(\tau)$ is obtained by interchanging the subscripts 1 and 2 and changing the sign of ϵ.

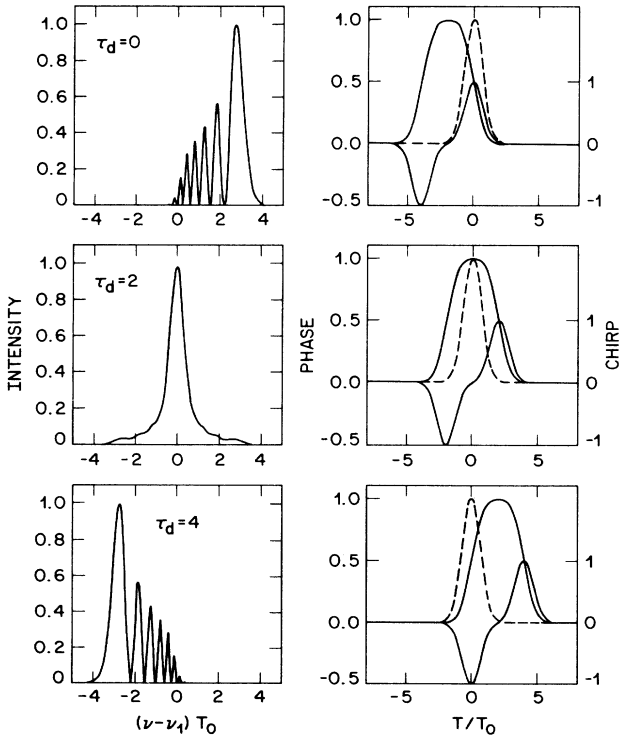

FIG. 1. Pulse spectra (left column) and XPM-induced phase and chirp (right column) for a probe pulse copropagating with a faster-moving pump pulse. The Gaussian pulse shape $|A_1(0,\tau)|^2$ is shown by a dashed line. The three rows correspond to an initial time delay of the pump pulse such that $\tau_d=0$, 2, and 4. Other parameters are $\gamma_1 P_2 L=40$ and $L/L_W=4$. The vertical scale is normalized to 1 in all cases.

The XPM contribution to the frequency chirp depends on the initial time delay τ_d between the two pulses. As a result, the pulse spectrum at the fiber output can exhibit qualitatively different features depending on the value of τ_d. The left column of Fig. 1 shows the spectra of pulse 1 for $\tau_d=0$, 2, and 4 whereas the right column shows the phase $\phi_1(\tau)$ and the frequency chirp $\Delta\nu_1(\tau)$. To isolate the features associated with the XPM, the SPM contribution is neglected by assuming $P_1 \ll P_2$. This would be the case in a pump-probe experimental configuration. For definiteness the pump pulse is assumed to travel faster than the probe pulse ($\epsilon=-1$). In the normal-dispersion regime this amounts to assuming that $\omega_1>\omega_2$. The fiber length $L=4L_W$ and the pump power is chosen such that $\gamma_1 P_2 L=40$ in Fig. 1.

The dependence of the probe spectra on the relative time delay can be understood by considering the XPM-induced chirp shown in the right column of Fig. 1. For $\tau_d=0$, the slow-moving probe pulse interacts mainly with the trailing edge of the pump pulse. As a result, the XPM-induced chirp is positive across the entire probe pulse, and the probe spectrum has only blue-shifted components. When $\tau_d=4$, the pump pulse just catches up with the probe pulse at the fiber output. Since it is the leading edge of the pump that interacts with the probe pulse, the chirp is negative, and the probe spectrum has only red-shifted components. When $\tau_d=2$, the pump passes through the probe pulse in a symmetric manner. As a result, the probe spectrum is symmetrically broadened. As shown in Fig. 1, the XPM-induced chirp is nearly linear across the probe pulse for $\tau_d=2$, a feature similar to the case of SPM. However, the magnitude of chirp is relatively small in the XPM case and depends on the ratio L/L_W.

The effect of initial time delay on the probe spectrum were first observed in a pump-probe experiment[9] where the effective initial delay was varied using time-dispersion tuning in a fiber-Raman laser. We have performed a different experiment[14] in which 1.06-μm pump pulses and 0.53-μm probe pulses are launched simultaneously in a 1-m-long fiber. The initial delay between the two pulses was adjusted using a Mach-Zehnder-interferometer delay line. The experiment allowed us to verify the nonlinear chirp model dicussed above. Because of a relatively large group-velocity mismatch ($\simeq$80 ps/m) between the pump and probe pulses, the walk-off length for pump pulses ($T_0\simeq 20$ ps) was only about 25 cm. Because of a relatively small interaction length, the probe spectrum was only slightly broadened and its internal structure could not be resolved. The peak of the spectrum was, however, shifted by an amount that depended both on the pump power P_2 and the relative delay τ_d. Such a shift can be referred to as the XPM-induced wavelength shift.[14] Figure 2 shows the induced wavelength shift as a function of τ_d. The solid line is the theoretical fit to the data and was obtained from Eq. (3.9) as follows. If we neglect the SPM contribution ($P_1 \ll P_2$), Eq. (3.9) becomes

$$\Delta\nu_1(\tau)=-\epsilon\Delta\nu_{\max}\{\exp[-(\tau-\tau_d)^2] - \exp[-(\tau-\tau_d-\epsilon L/L_W)^2]\} , \quad (3.10)$$

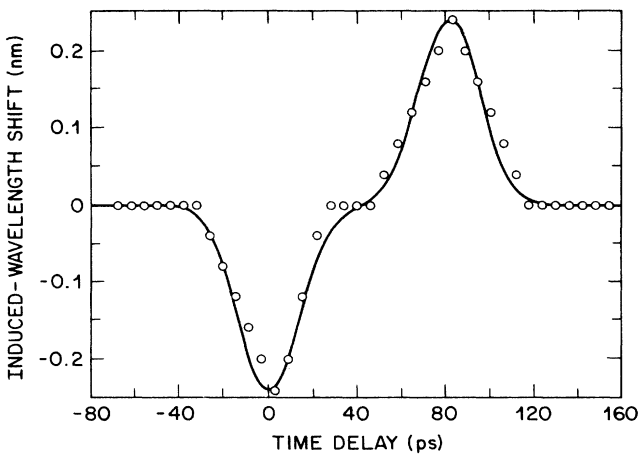

FIG. 2. XPM-induced wavelength shift of a 0.53-μm probe pulse as a function of the initial time delay of 1.06-μm pump pulse. Open circles shown the experimental data, while the solid line shows the theoretical prediction.

where

$$\Delta\nu_{\max}=\gamma_1 P_2 L_W/(\pi T_0) \ . \tag{3.11}$$

The induced frequency shift for a given τ_d is obtained by maximizing $|\Delta\nu_1(\tau)|$. The maximum occurs near $\tau=0$. The theoretical fit in Fig. 2 is obtained from Eq. (3.10) by setting $\tau=0$, $\epsilon=-1$, $L/L_W=4$, and $T_0=20$ ps. The good agreement indicates the usefulness of the simple model used to derive Eq. (3.9).

IV. DISPERSIVE CROSS-PHASE MODULATION

As discussed in Sec. III, when $L_D \gg L_W$, the XPM broadens the pulse spectrum asymmetrically but the pulse shape remains unchanged. If L_D becomes comparable to L_W, the combined effects of XPM and GVD can lead to qualitatively new temporal changes that accompany the spectral changes. In this section we study these changes by solving Eqs. (2.14) and (2.15) numerically. It is useful to introduce the normalized distance ξ and the normalized amplitudes U_1 and U_2 as

$$\xi=z/L_D, \quad U_j=A_j/\sqrt{P_1} \ , \tag{4.1}$$

where $j=1$ or 2. Equations (2.14) and (2.15) then take the form

$$\frac{\partial U_1}{\partial\xi}+\frac{i}{2}\mathrm{sgn}(\beta_1)\frac{\partial^2 U_1}{\partial\tau^2}=iN^2(|U_1|^2+2|U_2|^2)U_1 \ , \tag{4.2}$$

$$\frac{\partial U_2}{\partial\xi}+\epsilon\frac{L_D}{L_W}\frac{\partial U_2}{\partial\tau}+\frac{i}{2}\frac{\beta_2}{|\beta_1|}\frac{\partial^2 U_2}{\partial\tau^2} =iN^2\frac{\omega_2}{\omega_1}(|U_2|^2+2|U_1|^2)U_2 \ , \tag{4.3}$$

where

$$N^2=\gamma P_1 L_D=\frac{\gamma_1 P_1 T_0^2}{|\beta_1|} \ . \tag{4.4}$$

The parameter N is related to the soliton order in the anomalous-GVD regime. It serves a useful purpose in the normal-GVD regime also in as much as it is a measure of the relative importance of the nonlinear effects.

Equations (4.2) and (4.3) can be used to describe the XPM interaction between two pulses of arbitrary peak powers by including the effects of SPM, XPM, GVD, and the pulse walk-off. To isolate the XPM effects, it is useful to consider a pump-probe configuration. If the pulse 1 is much more intense than pulse 2, one can neglect $|U_2|^2$ on the right-hand side of Eqs. (4.2) and (4.3). Equation (4.2) then reduces to the conventional nonlinear Schrödinger equation. It governs the evolution of the pump pulse which travels unaffected by the presence of the probe pulse. Equation (4.3) describes probe evolution along the fiber length in the presence of the XPM and GVD effects. Figures 3 and 4 show the evolution of the shape and the spectrum of the probe pulse for the case $N=10$, $L_D/L_W=10$, $\omega_2/\omega_1=1.2$, and $\beta_1\simeq\beta_2>0$. The pump and probe pulses are taken to be Gaussin of the same width with no initial time delay ($\tau_d=0$) at the fiber input. The pump pulse is assumed to travel faster than the probe pulse ($\epsilon=1$). Both pulses are assumed to propagate in the normal-GVD regime of the fiber.

The most notable effect of GVD is related to the shape of the probe pulse in Fig. 3. In the absence of GVD, the pulse shape would remain unchanged. However, when the GVD effects are important, the pulse broadens, becomes asymmetric, and develops considerable internal structure. The origin of the asymmetry and the oscillatory structure on the trailing side is related to the XPM-induced chirp given by Eq. (3.9). As seen in the top row of Fig. 1, the chirp is positive across the entire pulse with the maximum occuring at the pulse center. As a result, the blue-shifted peak of the probe pulse travels slower than the wings as it propagates down the fiber. Since the peak lags behind, it interferes with the trailing edge. The

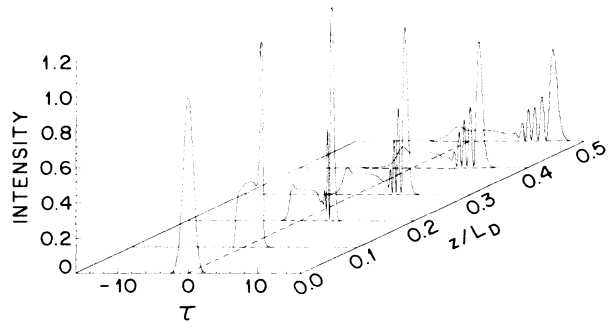

FIG. 3. Evolution of the probe pulse along the fiber for $N=10$, $L_D/L_W=10$, $\omega_2/\omega_1=1.2$, and $\tau_d=0$. The intensity $|U_2(\xi,\tau)|^2$ is plotted for ξ in the range 0–0.5. Both pump and probe pulses are taken to be Gaussian and propagate in the normal-dispersion regime of the fiber. The peak intensity at $\xi=0$ is normalized to 1 ($\xi=z/L_D$).

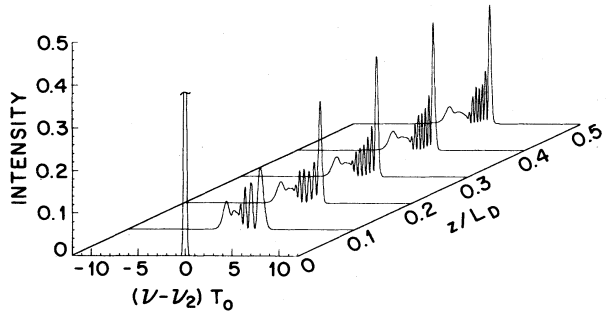

FIG. 4. Evolution of the probe spectrum corresponding to the pulse shapes of Fig. 3. The spectral intensity $|\tilde{U}_2|^2$ is plotted, where $\tilde{U}_2$ is the Fourier transform of U_2. The peak intensity at $z=0$ is normalized to 1.

rapid oscillations on the trailing side in Fig. 3 are due to such an interference. This behavior is similar in nature to the phenomenon of optical-wave breaking occuring as a result of dispersive SPM when a single intense pulse propagates in the normal-GVD regime of a fiber. It can be referred to as the XPM-induced optical-wave breaking.[19]

In spite of the identical nature of the underlying physical mechanism, optical-wave breaking exhibits different qualitative features in the case of XPM when compared with the SPM case. The most striking difference is that the pulse shape is asymmetric with only one edge developing oscillations. For the case shown in Fig. 3, oscillations occur near the trailing edge because of the faster-moving pump pulse interacts mainly with the trailing edge. If the probe and pump wvelengths were reversed, oscillations would occur near the leading edge. This can also be understood by noting that in that case the XPM-induced chirp is negative. Consequently, the red-shifted peak of the probe pulse travels faster than the wings and interferes with the leading edge. In fact, the shape and the spectrum of the probe pulse are just the mirror images of those shown in Fig. 3 if the wavelengths are interchanged while keeping all other parameters the same.

The results shown in Fig. 3 correspond to the case in

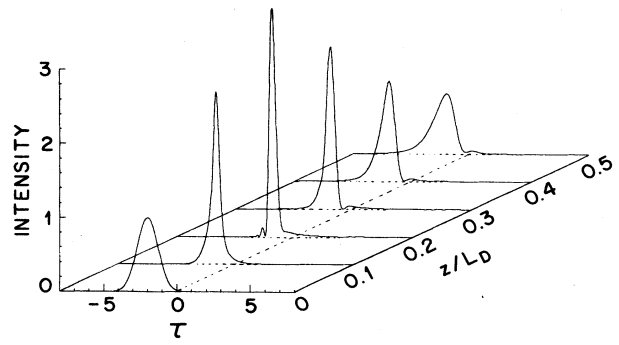

FIG. 5. Evolution of the probe shape for parameter values indentical to those used in Fig. 3 except that $\tau_d=-2$.

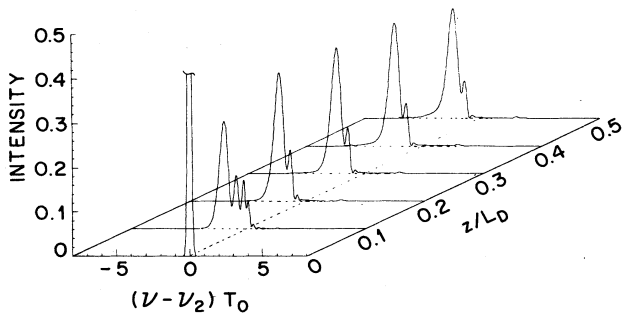

FIG. 6. Evolution of the probe spectrum corresponding to the pulse shapes shown in Fig. 5.

which the pump and probe pulses are launched without any initial delay between them ($\tau_d=0$). Similar to the case of nondispersive XPM shown in Fig. 1, the probe evolution can exhibit a qualitatively different behavior when $\tau_d\neq 0$. Figure 5 shows evolution of the probe pulse under conditions identical to those of Fig. 3 except that $\tau_d=-2$, i.e., the probe pulse is initally advanced by $2T_0$ with respect to the pump pulse. The corresponding probe spectra are shown in Fig. 6. It is evident that evolution of the probe pulse is influenced considerably by the initial time delay. In particular, in contrast to the $\tau_d=0$ case where the probe pulse experiences broadening, the probe pulse is compressed during the early stages of propagation. The maximum compression (by about a factor of 4) occurs near $\xi=0.2$ or $z=2L_W$. The probe pulse starts to rebroaden with further propagation.

The probe evolution can be understood by considering the XPM-induced chirp. Strictly speaking, the chirp model of Sec. III is not applicable since the shape of the pump pulse changes considerably along the fiber length. Nonetheless, it can be used for the early stages of pulse evolution. For $\xi \lesssim 0.2$, the pump pulse interacts mainly with the trailing edge of the probe pulse and generates a negative chirp. The trailing edge of the probe pulse then consists of red-shifted spectral components which travel faster than the leading edge in the presence of positive GVD. This leads to a compression of the trailing edge of the probe pulse seen clearly in Fig. 5. In the mean time the pump pulse broadens considerably. Since the pump power becomes relatively constant over the entire probe pulse, the XPM-induced frequency chirp is reduced. The probe pulse then starts to broaden beyond $\xi \geq 0.2$, as one would expect in the normal-GVD regime of the fiber. However, it travels faster than the group velocity associated with it at the fiber input. This increase in the group velocity is due to the XPM-induced spectral shift apparent in Fig. 6. Since the probe spectrum is shifted toward red, the effective group velocity becomes larger in the case of normal GVD. The opposite would happen if the probe pulse were to experience anomalous GVD.

V. PULSE COMPRESSION

An important application of the fiber nonlinearity is for pulse compression.[27] When a single optical pulse propagates through a fiber, the nonlinear phenomenon of

SPM imposes a nearly linear positive chirp (frequency increases with time) on it, and the pulse can be compressed by passing it through a dispersive delay with anomalous (or negatve) GVD. A grating pair is generally used for this purpose in the visible and near-infrared regions whereas a fiber can be used for wavelengths exceeding 1.3μm. In the latter case, the same piece of fiber can provide the chirp and the compression. Such a scheme is sometimes referred to as the soliton-effect compression scheme since it takes advantage of the periodic evolution of the higher-order solitons.[27] Both the fiber-grating and soliton-effect compression techniques require that the energy of the input pulses be relatively large ($\gtrsim 100$ pJ) and cannot be used to compress weak optical pulses.

The nonlinear phenomenon of XPM has the potential for compressing weak-picosecond and -femtosecond pulses since an intense pump pulse can be used to impose the chirp on the weak probe pulse.[17–19] As seen in Fig. 1, the XPM-induced chirp is affected by pulse walk-off and depends critically on the initial relative pump-probe delay. Clearly the use of XPM for pulse compression would require a careful control of the pump-pulse parameters such as its width, peak power, wavelength, and synchronization with the probe pulse.

Two cases must be distinguished depending on the relative magnitudes of the walk-off length L_W and the dispersion length L_D. If $L_D \gg L_W$ throughout the propagation, the GVD effects are negligible. In that case the fiber is used to impose a chirp on the probe pulse through XPM, and an external grating pair is needed to compress it. The results of Sec. II can be used to analyze the magnitude and the form of the chirp in this case of nondispersive XPM. The results show[17] that a nearly linear positive chirp can be imposed across the probe pulse when the pump pulse is much wider than the probe pulse. The case in which L_D and L_W are comparable ($L_D \lesssim 10L_W$) is of considerable interest since the same piece of fiber can be used to impose the chirp and to compress the pulse. Furthermore, in contrast with the SPM case where such single-stage compression occurs only in the anomalous-GVD region ($\lambda > 1.3$ μm), the XPM offers the possibility of single-stage compression even in the visible region without the need of a grating pair. In the following, we discuss XPM-induced pulse compression in the normal and anomalous GVD regimes separately.

Consider first the case in which both the pump and probe pulses propagate in the normal-GVD regime of the fiber. Figure 5 shows the probe-pulse evolution for a specific set of pump-pulse parameters, namely, $N=10$, $L_D/L_W=10$, $\lambda_1/\lambda_2=1.2$, $T_0=T_1=T_2$, and $\tau_d=-2$. The probe pulse is compressed by about a factor of 4 at $z=2L_W$. In general, the compression quality, the compression factor, and the optimum fiber length depend on several input parameters such as the pump-probe wavelength difference, the pump-probe width ratio, the pump peak power, and the initial pump-probe delay τ_d. The dependence on the last parameter is particulary important since τ_d can be adjusted in practice to optimize the compressor performance. To understand this dependence, we have performed numerical simulations for a wide range of τ_d while keeping the other parameters the same. The maximum compression occurs at a distance.

$$z_{\max} \simeq |\tau_d| L_W = \frac{T_d}{|v_{g_1}^{-1} - v_{g_2}^{-1}|} . \tag{5.1}$$

It corresponds to a distance at which the two pulses would catch up in the absence of the GVD effects. The maximum compression may, however, not be desirable from the standpoint of the compression quality. This is apparent in Fig. 5 where the compressed pulse has an oscillatory structure (ringing) near the leading edge and a broad pedestal near the trailing edge at $z=z_{\max}$ ($\xi=0.2$); these features are undesirable from the quality standpoint. In fact, the pulse at $\xi=0.1$ appears to be of higher quality even though the compression factor is lower than that at $\xi=0.2$. The main point is that a tradeoff exists between the magnitude and the quality of compression and that the fiber length can be chosen to meet the particular need.

The relative pump-probe delay τ_d affects the compression quality in a subtle way. For $|\tau_d| \lesssim 2$, the maximally compressed pulse has less riging near the leading edge but contains more energy in the trailing-edge pedestal. For $|\tau_d| \gtrsim 2$, the pedestal nearly disappears while the ringing becomes more dominant. For the parameters of Fig. 5, $|\tau_d|$ in the 2–2.5 range appears to be optimum. Figure 7 shows the input pulse and the compressed pulse at $\xi=0.2$ for $\tau_d=-2.5$, while other parameters are indentical to those of Fig. 5. The pulse is compressed by about a factor of 4 and does not have a pedestal on the trailing side. Except for some ringing on the leading side, the compressed pulse is of high quality. Even this ringing can be removed if the pump pulse is initially wider than the probe pulse, although only at the expense of reduction in the amount of compression achievable at a given pump power. The main conclusion is that XPM and GVD can be used to compress weak probe pulses in normal-dispersion region of the optical fiber by optimiz-

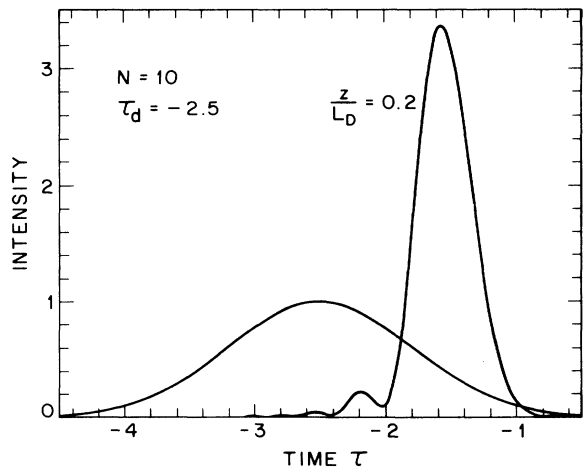

FIG. 7. Compressed probe pulse at $\xi=0.2$ ($z=2L_W$) for the case $\tau_d=-2.5$. The input probe pulse at $\xi=0$ is also shown for comparison.

ing the width and the initial delay of the pump pulse. The compression factor is in the 3–5 range for $N=10$ but can be increased by increasing the pump-peak power (so that N is larger). We also investigated the case in which the pump pulse travels slower than the probe pulse and is advanced initially ($\lambda_1 < \lambda_2$, $\tau_d > 0$). The qualitative behavior remains the same.

When both the pump and probe pulses propagate in the normal-dispersion regime, the compressed pulse is necessarily asymmetric because of the group-velocity mismatch and the associated walk-off effects. The walk-off effects can be considerably reduced if the pump and probe wavelengths are chosen to be on the opposite sides of the zero-dispersion wavelength of the fiber ($\lambda_D \simeq 1.3$ μm). One posibility consists of using the 1.06-μm pump pulses for compressing the probe pulses near 1.55 μm (obtained, for example, from a mode-locked semiconductor laser). The probe pulse by itself is too weak to propagate as a fundamental or higher-order soliton. However, the XPM-induced chirp imposed on it by the copropagating pump pulse may be strong enough that the probe pulse goes through an initial compression phase associated with the higher-order solitons. This case has recently been considered.[18] Here we focues on the optimization issues.

Figures 8 and 9 show the evolution of the shape and the spectrum of 1.55-μm probe pulses launched together with the 1.06-μm pump pulses whose peak power is such that the parameter $N=10$. For simplicity, the group velocity for the pump and probe pulses is assumed to be the same. Furthermore, the two pulses are launched without initial time delay so that they overlap initially and continue to do so during their passage through the fiber. The inclusion of walk-off effects does not affect the qualitative behavior as long as the walk-off length is much larger than the dispersion length ($L_W \gg L_D$).

The most notable feature of Fig. 8 is the initial compression of the probe pulse before the pulse broadens and splits into several components. At $\xi=0.1$ the probe pulse is compressed by about a factor of 4. The compression factor increases to 6 at $\xi=0.2$ but the pulse develops

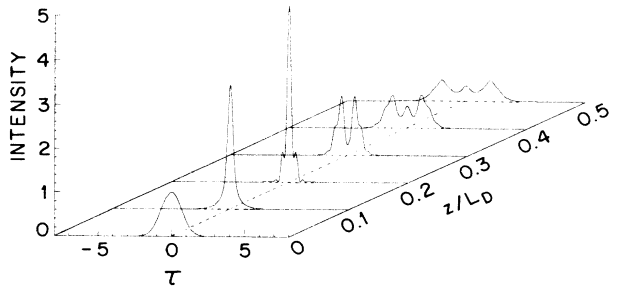

FIG. 8. Evolution of the probe shape for the case in which the pump and probe pulses experience normal and anomalous GVD, respectively, are launched without any initial time delay ($\tau_d=0$), have the same width ($T_1=T_2=T_0$), and propagate inside the fiber with the same group velocity. The parameter $N=10$.

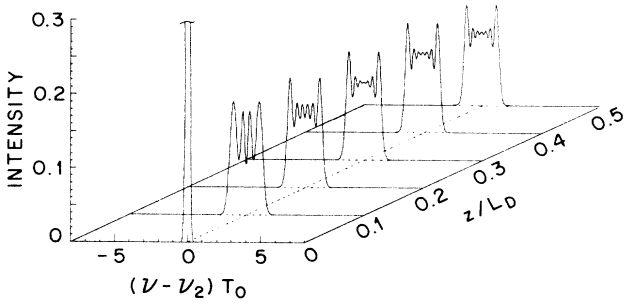

FIG. 9. Evolution of the probe spectrum under conditions identical to those of Fig. 8.

side lobes in the wings. With further propagation, the probe pulse splits into three components which broaden rapidly with the propagated distance. This behavior can be understood by considering the XPM-induced chirp. During the initial stages of probe evolution, the pump pulse induces a chirp on the probe pulse through XPM. The chirp features are similar to that induced by SPM. In particular, the chirp is nearly linear over the central part of the probe pulse. The anomalous GVD compresses the central part, as seen in Fig. 8 for $\xi=0.1$. In the mean time, the pump pulse broadens considerably as a result of normal GVD experienced by it. The XPM-induced chirp then nearly vanishes across the entire probe pulse. This is evident in Fig. 9 where the probe spectrum ceases to change beyond $\xi \geq 0.3$. The probe pulse then evolves as if the pump pulse did not exist. However, the spectral changes produced by the pump during the early stages modify the probe shape considerably. In particular, the energy in the red-shifted and the blue-shifted components separates from the central peak as a result of their slightly different group velocities. This results in the three-peak shape seen in Fig. 8 beyond $\xi \geq 0.4$.

It is evident from Fig. 8 that the probe pulse can be compressed considerably if the fiber length is suitably chosen. Similar to the case of Fig. 5, a tradeoff exists between the compression quality and the amount of compression for a given pump power. For the case

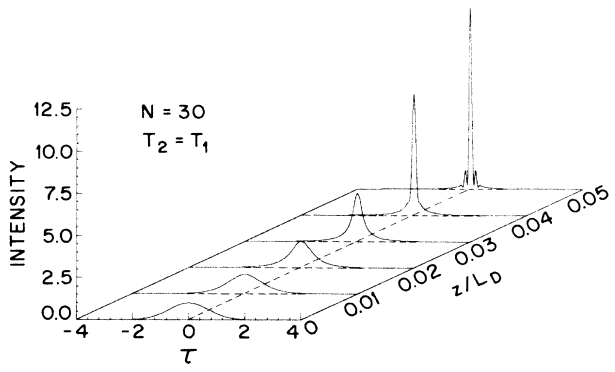

FIG. 10. Probe evolution under conditions identical to those of Fig. 8 except that $N=30$.

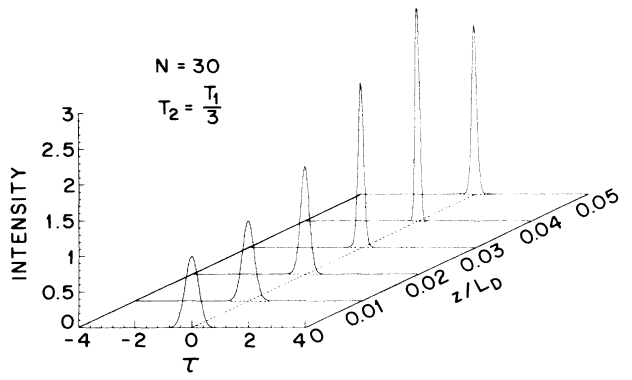

FIG. 11. Probe evolution under conditions identical to those of Fig. 10 except that the probe pulse is shorter than the pump pulse by a factor of 3.

$N=10$ shown in Fig. 8, the probe pulse can be compressed by a factor of about 4 at $z/L_D=0.1$ with a high quality. Higher compression factors can be obtained by increasing the pump power. Figure 10 shows the probe evolution under identical conditions except that the pump power has been increased by a factor of 9 ($N=30$). Good quality compression by a factor of about 10 occurs for z/L_D in the vicinity of 0.04. Compression by a factor of more than 15 is possible for $z/L_D \simeq 0.05$ but the quality is not as good.

The above results were obtained by assuming that the input widths of the pump and probe pulses are the same ($T_1=T_2=T_0$). We have carried out extensive numerical calculations for various pump-probe width ratios to understand the role of different pulse widths. When the pump pulse is shorter than the probe pulse, the compression factor is larger but the pulse quality is poorer as the pulse rides on a broad pedestal. This can be understood by noting that for short pump pulses the XPM-induced chirp is linear only over a small central part of the probe pulse. By the same token, the compression quality can be improved when the pump pulse is broader than the probe pulse, but only at the expense of a reduction in the amount of compression realized at a given pump power. Figure 11 illustrates this situation for the case $T_2=T_1/3$ i.e., the pump pulse is broader by a factor of 3. All other parameters are identical to those of Fig. 10. The main conclusion is that the pump-probe width ratio is a critically important parameter that determines the quality and the amount of compression that can be realized for a given pump power.

VI. CONCLUSIONS

This paper has focused on the temporal and spectral changes that a probe pulse can experience when it is launched into an optical fiber together with an intense pump pulse. The changes occur as a result of the fiber nonlinearity which couples the two pulses through the nonlinear phenomenon of XPM. The XPM-induced coupling occurs irrespective of the wavelength difference between the two pulses. The fiber length over which such a coupling occurs, however, depends on the walk-off length which in turn depends on the respective wavelengths and their relation to the zero-dispersion wavelength of the fiber.

The XPM effects can be divided into two categories depending on whether the GVD effects are important or not during the XPM interaction. If the dispersion length is much larger than the walk-off length, the pulse shape remains nearly unchanged while the XPM-induced chirp can broaden and distort the probe spectrum. The initial time delay between the pump and probe plays an important role in determining the spectral changes. If the dispersion length and the walk-off length become comparable, the pulse shape also changes during the XPM interaction. The temporal changes also depend on the initial delay between the pump and probe pulses. When the two pulses are launched simultaneously, XPM can induce optical wave breaking that manifests as rapid oscillations near the leading or the trailing edge of the probe pulse. Physically, the peak of the probe pulse travels either faster or slower than the wings by an amount that depends on the peak intensity of the pump pulse.

XPM can be used to compress a weak probe pulse by copropagating it together with an intense pump pulse. We have discussed two modes of operation in which the combination of XPM and GVD can compress weak probe pulses. For visible and near-infrared probe pulses, the initial pump-probe delay need to optimized whereas the pump and probe wavelengths should not be too different to increase the interaction length. For probe pulses at wavelengths exceeding 1.3 μm, the pump-pulse wavelength is chosen in the normal-dispersion regime to match the group velocities of the two pulses approximately. Furthermore, the two pulses are launched in a synchronized manner. The latter technique has the potential for practical applications since it can be used to enhance the peak power of pulses obtained from mode-locked semiconductor lasers. In particular, the 1.55-μm probe pulses can be compressed by using 1.06-μm pump pulses.

ACKNOWLEDGMENTS

The research at City College of New York is supported in part by Hamamatsu Photonics K.K. The work at the University of Rochester is partially supported by the Joint Services Optics Program.

[1]M. A. Duguay, in *Progress in Optics*, edited by E. Wolf (North-Holland, Amsterdam, 1976), Vol. 14, p. 163.
[2]R. W. Hellwarth, Prog. Quantum Electron. **5**, 1 (1977).
[3]Y. R. Shen, *The Principles of Nonlinear Optics* (Wiley, New York, 1984), Chap. 16.
[4]R. H. Stolen and A. Ashkin, Appl. Phys. Lett. **22**, 294 (1973).
[5]J. I. Gersten, R. R. Alfano, and M. Belic, Phys. Rev. A **21**, 1222 (1980).

[6]A. R. Chraplyvy and J. Stone, Electron. Lett. **20**, 996 (1984).
[7]R. R. Alfano, Q. X. Li, T. Jimbo, J. T. Manassah, and P. P. Ho, Opt. Lett. **14**, 626 (1986).
[8]D. Schadt, B. Jaskorzynska, and U. Osterberg, J. Opt. Soc. Am. B **3**, 1257 (1986); D. Schadt and B. Jaskorzynka, *ibid.* **4**, 856 (1987).
[9]M. N. Islam, L. F. Mollenauer, R. H. Stolen, J. R. Simpson, and H. T. Shang, Opt. Lett. **12**, 625 (1987).
[10]R. R. Alfano, P. L. Baldeck, F. Raccah, and P. P. Ho, Appl. Opt. **26**, 3491 (1987).
[11]G. P. Agrawal, Phys. Rev. Lett. **59**, 880 (1987).
[12]J. T. Manassah, Appl. Opt. **26**, 3747 (1987).
[13]R. R. Alfano and P. P. Ho, IEEE J. Quantum Electron. **QE-24**, 351 (1988).
[14]P. L. Baldeck, R. R. Alfano, and G. P. Agrawal, Appl. Phys. Lett. **52**, 1939 (1988).
[15]P. L. Baldeck, R. R. Alfano, and G. P. Agrawal, in *Ultrafast Phenomena VI,* edited by T. Yajima, K. Yushihara, C. B. Harris, and S. Shinoya (Springer-Verlag, Berlin, 1988), pp. 53–55.
[16]A. S. Gouveia-Neto, M. E. Faldon, A. S. B. Sombra, P. G. J. Wigley, and J. R. Taylor, Opt. Lett. **13**, 901 (1988).
[17]J. T. Manassah, Opt. Lett. **13**, 755 (1988).
[18]B. Jaskorzynska and D. Schadt, IEEE J. Quantum Electron. **QE-24**, 2117 (1988).
[19]G. P. Agrawal, P. L. Baldeck, and R. R. Alfano, Opt. Lett. **14**, 137 (1989).
[20]S. Trillo, S. Wabnitz, E. M. Wright, and G. I. Stegeman, Opt. Lett. **13**, 871 (1988).
[21]S. Chi and S. Wen, Opt. Lett. **14**, 84 (1989).
[22]F. Kh. Abdullaev, R. M. Abrarov, and S. A. Darmanyan, Opt. Lett. **14**, 131 (1989).
[23]See, for example, G. P. Agrawal, *Nonlinear Fiber Optics* (Academic, Boston, 1989), Chap. 7.
[24]R. M. Mitschke and L. F. Mollenauer, Opt. Lett. **11**, 659 (1986).
[25]J. P. Gordon, Opt. Lett. **11**, 662 (1986).
[26]Y. Kodama and A. Hasegawa, IEEE J. Quantum Electron. **QE-23**, 510 (1987).
[27]For a review, see Chap. 6 of Ref. 23.